Antigen-dependent inducible T cell reporter system for PET imaging of breast cancer and glioblastoma

Jaehoon Shin[1,12], Matthew F. L. Parker[1,11,12], Iowis Zhu[2,3,12], Aryn Alanizi[1], Carlos I. Rodriguez[4], Raymond Liu[2,3], Payal B. Watchmaker[5], Mausam Kalita[1], Joseph Blecha[1], Justin Luu[1], Brian Wright[6], Suzanne E. Lapi[6], Robert R. Flavell[1,7], Hideho Okada[3,5,7], Thea D. Tlsty[4]*, David M. Wilson[1]* & Kole T. Roybal[2,3,7-10]*

[1] Department of Radiology and Biomedical Imaging, University of California, San Francisco, San Francisco, CA, USA
[2] Department of Microbiology and Immunology, University of California, San Francisco, San Francisco, CA, USA
[3] Parker Institute for Cancer Immunotherapy, San Francisco, CA, USA
[4] Department of Pathology, University of California, San Francisco, San Francisco, CA, USA
[5] Department of Neurological Surgery, University of California, San Francisco, CA, USA
[6] Department of Radiology, University of Alabama at Birmingham, AL, USA
[7] Helen Diller Cancer Center, University of California, San Francisco, San Francisco, CA, USA.
[8] Chan Zuckerberg Biohub, San Francisco, CA, USA
[9] Gladstone UCSF Institute for Genetic Immunology, San Francisco, CA, USA
[10] UCSF Cell Design Institute, San Francisco, CA, USA
[11] Current address: Department of Psychiatry, Renaissance School of Medicine at Stony Brook University, Stony Brook, NY, USA
[12] These authors contributed equally: Jaehoon Shin, Matthew F. L. Parker, Iowis Zhu
* email: kole.roybal@ucsf.edu, david.m.wilson@ucsf.edu, thea.tlsty@ucsf.edu

*Correspondence and Reprint Request:

Kole T. Roybal, Ph.D.
Department of Microbiology and Immunology
University of California, San Francisco
505 Parnassus Ave.
San Francisco, CA 94143
Phone: (415) 476-8289
Kole.Roybal@ucsf.edu

David M. Wilson, M.D., Ph.D.
Department of Radiology and Biomedical Imaging
University of California, San Francisco
505 Parnassus Ave.
San Francisco, CA 94143
Phone: (415) 353-1668
david.m.wilson@ucsf.edu

Thea D. Tlsty, Ph.D.
Department of Pathology
University of California, San Francisco
505 Parnassus Ave.
San Francisco, CA 94143
Phone: (415)502-6116
thea.tlsty@ucsf.edu

Running title: Antigen-inducible SNIPR-PET reporter system

Keywords: synNotch, SNIPR, CAR-T, positron emission tomography, reporter, cancer antigens, HER2, EGFRvIII

Acknowledgements: Grant sponsors NIH (R01-EB024014, R01-EB025985); Kleberg Foundation 132472B; Society of Interventional Radiology.

Abstract: For the past several decades, chimeric antigen receptor T cell (CAR T) therapies have shown promise in the treatment of cancers. These treatments would greatly benefit from companion imaging biomarkers to follow the trafficking and activation of T cells *in vivo*. Using synthetic biology, we engineered T cells with a chimeric receptor SyNthetic Intramembrane Proteolysis Receptor (SNIPR) that induces overexpression of an exogenous reporter gene cassette upon recognition of specific tumor markers. We then applied a SNIPR-based positron emission tomography (PET) reporter system to two cancer-relevant antigens, human epidermal growth factor receptor 2 (HER2) and epidermal growth factor receptor variant III (EGFRvIII), commonly expressed in breast and glial tumors respectively. Antigen-specific reporter induction of the SNIPR-PET T cells was confirmed *in vitro* using GFP fluorescence, luciferase luminescence, and the HSV-TK PET reporter with [^{18}F]FHBG. Tumors were successfully imaged using PET in dual xenograft HER2+/HER2- and EGFRvIII+/EGFRvIII- animal models, with > 10-fold higher [^{18}F]FHBG signals seen in antigen-expressing tumors versus the corresponding controls. The main innovation described is therefore PET detection of therapeutic T cells via specific antigen-induced signals, in contrast to reporter systems relying on constitutive gene expression.

Chimeric antigen receptor T cell (CAR T) therapy has revolutionized oncology, demonstrating promising results for refractory drug-resistant leukemias and lymphomas[1–3] among other cancers. CAR T cells are engineered to respond to cancer cells expressing a specific protein target, inducing rapid cell division and clonal expansion within the tumor microenvironment and activating immune response to target cells via local secretion of cytokines, interleukins, and growth factors[4,5] **(Fig. 1a)**. Hundreds of clinical trials have been initiated globally to study CAR T cells, with two of the most popular targets CD19[6], and BMCA (seen in multiple myeloma)[7,8]. There are several critical limitations of CAR T therapy, such as exhaustion and senescence by excessive antigen exposure and inability to predict the off-site activation. Importantly, there were engineered T cell clinical trials resulting in patient deaths due to off-target effects, which may have been mediated by recognition of normal lung[9] or cardiac[10,11] tissues. We currently do not have tools to detect the aberrant activation of CAR T cells *in vivo* prior to advanced tissue damage, which only can be identified via biopsy or autopsy. Non-invasive methods are therefore critical in evaluating the efficacy and safety of preclinical CAR T therapies and CAR T clinical trials by providing surrogate real-time maps for patient-specific and tumor-specific activation profiles.

Current limitations in predicting CAR T performance and safety *in vivo* are potentially addressed by the positron emission tomography (PET)-compatible SyNthetic Intramembrane Proteolysis Receptor (SNIPR) T cells described in this manuscript. The SNIPR system has produced a powerful new class of chimeric receptors that bind to target surface antigens and induce transcription of exogenous reporter genes via release of a transcription factor domain by regulated intramembrane proteolysis (**Fig. 1b**). Compared to its archetype synthetic Notch (synNotch) receptor[12–14], SNIPR can exhibit significantly greater reporter induction efficacy while maintaining minimal background activity[15]. This powerful technique can activate any genes of interest that are co-introduced. The SNIPR contains the regulatory transmembrane domain of human Notch receptor but bears an extracellular antigen recognition domain (eg. single-chain variable fragment or scFv) and an intracellular transcriptional activator domain (Gal4-VP64). When the SNIPR engages its target antigen on an opposing cell, this induces intramembrane cleavage, releasing the intracellular transcriptional domain Gal 4, allowing it to enter the nucleus to activate transcription of target genes. The SNIPR system has been applied to several solid human tumors with the potential to overcome numerous therapeutic challenges including heterogeneity and antigen escape[16,17].

Despite the great versatility of synNotch and SNIPR, their diagnostic potential has not yet been explored. Current PET approaches producing antigen-dependent signals are dominated by immunoPET, whereby a monoclonal antibody is labeled with a radioisotope such as [^{89}Zr][18–20]. In the described SNIPR approach, PET signals also depend on the interaction between an antigen and its corresponding scFv, but occur via T cell-based overexpression of the HSV-TK reporter. Recently, Aalipour *et al.* successfully demonstrated cell-based imaging for high sensitivity tumor detection[21]. The Gambhir group engineered macrophages to couple reporter expression to the activation of the arginase-1 promoter, which is specifically active in M2 tumor-associated macrophages. Using luciferase as a reporter, the authors were able to image tumors as small as 25–50 mm^3 in mice. While promising, information acquired from this strategy is limited by nonspecific distribution of M2 macrophages in many different types of tumors and non-neoplastic conditions such as fungal infection or tissue fibrosis[22,23]. Luciferase imaging is also limited by poor tissue penetration, so cannot be used in most human cancer detection[24,25].

In this manuscript, we combined CAR and SNIPR technologies to develop a new T cell-based molecular sensor that can image activated CAR T cells in action. Upon binding an antigen target, CAR produces rapid T cell division within the tumor microenvironment while SNIPR activates the over-expression of PET-imaging reporter genes. We developed HER2 and EGFRvIII-specific SNIPR T-cells that were successfully imaged *in vivo* upon interaction with their corresponding antigen-expressing tumors. We also compared HER2-specific SNIPR T cells to the “naked” [^{89}Zr]-modified anti-HER2 monoclonal antibody ([^{89}Zr]herceptin) used in immunoPET to validate the specificity of the cell-based method. These studies provide the foundation for applying the SNIPR-PET reporter to a variety of T cell-based therapies.

Results:

***Synthesis and in vitro validation of PET-compatible antiHER2-SNIPR T cells*.** To investigate the SNIPR-PET imaging approach, we started with one of the most extensively studied tumor antigens HER2, an extensively studied tumor antigen[14]. Following the published protocol by Roybal et al.[14], we transduced human CD4+ T cells with two plasmids encoding a SNIPR containing an anti-HER2 scFv (4D5-8), and an inducible reporter. For anti-HER2 SNIPR, we used the SNIPR with an anti-HER2 scFv binding head, an optimized truncated CD8α hinge region, human Notch1 transmembrane domain, intracellular Notch2 juxtamembrane

domain, and a transcriptional element composed of GAL4-VP64[26] (**Fig. 2a**). For the reporter, we used SR39 mutant herpes simplex virus-thymidine kinase (HSV1-sr39tk)-GFP fusion protein and enhanced firefly luciferase (fLuc)[27–29]. HSV1-thymidine kinase (HSV-tk) is an extensively studied reporter gene that has been used for imaging and gene therapy[30,31]. Unlike mammalian thymidine kinases, HSV-tk has promiscuous activity for various purine- or pyrimidine-derived nucleoside analogues, including the PET tracer 9-(4[^{18}F]fluoro-3-hydroxymethylbutyl) guanine ([^{18}F]FHBG), thereby retaining them within cells. In this manuscript, we used the hyperactive mutant HSV1-sr39tk to maximize the detection sensitivity[28,32] (**Supp. Fig. S1a**). When evaluating tk reporter expression upon SNIPR activation, HSV1-sr39tk-GFP fusion protein was used instead for ready assessment using flow cytometry (**Supp. Fig. S1b, top**). In all the subsequent radiotracer uptake experiments, however, HSV1-sr39tk was cloned with self-cleavage sequence T2A followed by super IL-2 (sIL-2) instead for higher level of T cell activation upon SNIPR activation (**Supp. Fig. S1b, bottom**). The level of fLuc enzymatic activity upon SNIPR activation was measured by luminometer after adding luciferin to the media.

We tested the induction of reporters including inducible HSV1-sr39tk-GFP and inducible luciferase activity, in the anti-HER2 SNIPR system (**Fig. 2a**). The newly synthesized anti-HER2 SNIPR T cells had comparable transduction efficacy to others we recently published[14] (**Fig. 2b**). Anti-HER2 SNIPR T cells were co-cultured with HER2+ breast cancer line SKBR3 and HER2– breast cancer line MD468 for 48 hours to induce SNIPR activation and downstream reporter gene expression (**Fig. 2c**). First, SNIPR activation induced over 160-fold expression of HSV1-sr39tk-GFP compared to negative control ($n=4$, $p < 0.001$) (**Fig. 2d**). Next, SNIPR activation induced over 30-fold higher luciferase activity compared to negative control ($n=4$, $p<0.001$) (**Fig. 2e**). Given that the anti-HER2 system is heavily optimized with scFv with high binding affinity scFvs and high antigen levels found on the target cells, we also tested scFvs with lower binding affinities and cancer cells with lower antigen abundance ($n = 3$ per combination). As expected, HSV1-sr39tk-GFP induction was correlated with both SNIPR binding affinity and antigen abundance (**Fig. 2f**). The induction of luciferase activity was also positively correlated with the target antigen abundance ($n=4$, one-way ANOVA $p<0.001$ for all comparisons of SKBR3)(**Fig. 2g**).

Activated antiHER2-SNIPR T cells show antigen-dependent [^{18}F]FHBG accumulation in vitro.

Human T cells require growth factors and cytokines to survive *in vitro* and *in vivo*[33]. One key cytokine is IL-2, which promotes the survival and clonal expansion of T cells[34]. Since human T cells do not have any growth factors or pro-survival cytokines in mice, we designed SNIPR T cells to secrete super IL-2 (sIL-2), upon binding to target antigens[35]. We created an inducible vector with HSV1-sr39tk and sIL-2, intervened by T2A self-cleaving peptides[36] (**Supp. Fig. S1b, bottom, Fig. 3a**). We induced the anti-HER2 SNIPR T cells by co-culturing them with SKBR3 or MD468 cells for 48 hours. [^{18}F]FHBG was added to the media and SNIPR T cells were incubated for 4 more hours (**Fig. 3b**). After removing the supernatant and washing, residual intracellular [^{18}F]FHBG was measured using a gamma counter. Anti-HER2 SNIPR T cells co-cultured with SKBR3 cells accumulated over 20-fold higher radiotracer levels compared to anti-HER2 SNIPR T cells co-cultured with MD468 cells (n = 3, p=0.013) (**Fig. 3c**). Once again, we tested [^{18}F]FHBG radiotracer uptake in suboptimal conditions by using scFvs with lower binding affinities and cancer cells with lower antigen abundance (n = 3 per combination). As expected, [^{18}F]FHBG incorporation was correlated with both SNIPR binding affinity and target antigen abundance (**Fig. 3d**).

Imaging using anti-HER2 SNIPR PET shows high antigen specificity in vivo.

Luciferase-based optical imaging: To investigate the feasibility of *in vivo* SNIPR-PET imaging, we initially studied luciferase induction in mice using time-dependent optical imaging. First, we found that 1 million MD468 (HER2+ breast cancer cell line, fast growing) and 3 million SKBR3 (HER2- breast cancer cell line, slow growing) subcutaneously injected xenografts generate roughly similar sized tumors in three weeks. We used anti-HER2 SNIPR T cells with inducible reporter fLuc-T2A-sIL-2 (**Supp. Fig. S2a**), analogous to HSV1-T2A-sIL-2 used in the *in vitro* study. The majority of tail vein injected SNIPR T cells localized to the spleen at day 3 and rapidly lost signal over time, likely due to insufficient pro-survival cytokines to stimulate survival/proliferation in mice (**Supp. Fig. S2c**). Since sIL-2 was not strong enough to induce T cell survival and proliferation *in vivo*, we introduced anti-HER2 CAR to the SNIPR T cells to more strongly induce T cell proliferation and survival as well as reporter (HSV1-sr39tk or fLuc) expression upon antigen binding (**Supp. Fig. S3a**). The FACS yield of T cell transduction with three plasmids was acceptable range, about 10% (**Supp. Fig. S3b**). In this system, anti-HER2 CAR is constitutively expressed, but only activates T cells and induces proliferation upon binding to its target antigen HER2. Of note, we used CD4+ T cells to minimize the target

killing activity with CAR activation. As a pilot experiment, we again generated similar sized SKBR3 (HER2+) and MB468 (HER2–) xenografts by subcutaneous injection, followed by anti-HER2 SNIPR T cell injection and bioluminescence imaging for the next 21 days (**Supp. Fig. S3c**). The luciferase-SNIPR T cell signal was much stronger within the HER2+ tumor, which is maximized at day 9, likely reflecting active proliferation within the tumor microenvironment (145 fold, no p value) (**Supp. Fig. S3d and e**). The signal, however, decreases over time afterwards, likely secondary to minimal target-killing activity of CD4, and clearing of target cells (**Supp. Fig. S3f**).

PET imaging: Based on the luciferase data, we generated SNIPR T cells with constitutively expressed anti-HER2 SNIPR and anti-HER2 CAR and conditionally expressed HSV-sr38tk-T2A-sIL2 (**Fig. 4a**). We first tested the efficacy of *in vitro* [^{18}F]FHBG uptake upon SNIPR activation in the SNIPR-CAR system, following the same experimental scheme as the SNIPR only system in **Fig. 3b.** As expected, when induced by co-culturing with SKBR3 (HER2+) cells, the SNIPR T cells accumulated 27-times higher amount of [^{18}F]FHBG than the SNIPR T cells co-cultured with MD468 (HER2–) cells (N = 8, p<0.001) (**Fig. 4b**). We also chose day 8 to image the SNIPR-T cells with anti-HER2 CAR and inducible HSV1-sr39tk-T2A-sIL2 in HER2+/HER2- xenograft model (**Fig. 4c**). Again, we generated similar sized HER2+(SKBR3) and HER2–(MB468) xenografts by subcutaneous injection into NCG mice, 4 weeks prior to the injection of SNIPR-CAR T cells with HSV-sr38tk-T2A-sIL2 reporter (N=7). [^{18}F]FHBG imaging was performed at 3, 6, 8 and 10 days by mPET-CT using an imaging protocol recently reported by our lab[37,38]. Encouragingly, greater [^{18}F]FHBG uptake on the HER2+ side compared to the HER2- side, indicating that the T cells localized around the HER2+ xenograft (n=7)**(Fig. 4d and e)**. There was an approximately 10-fold higher [^{18}F]FHBG uptake on HER2+ xenograft compared to HER2- xenograft ($p < 0.001$), and approximately 13-fold higher [^{18}F]FHBG uptake on HER2+ xenograft compared to shoulder muscle ($p < 0.001$), based on region of interest (ROI) analysis. In contrast, there was no significant difference in [^{18}F]FHBG signal between and background muscle ($p > 0.05$). As seen on SNIPR-CAR system with luciferase reporter in **Supp. Fig. S3e**, [^{18}F]FHBG signal decreased at 10 days post T cell IV injection, at which time, the tumors were harvested for ex vivo biodistribution analysis **(Fig. 4e)**. The difference of PET signal between HER2+ and HER2– xenografts was 5 fold with p=0.003 at day 10, and the difference of ex vivo radioactivity between HER2+ and HER2– xenograft was 4.2 fold with p=0.036 (**Fig. 4f, g**). Images from

the PET study showed marked radiotracer in the stomach, intestine, and gallbladder consistent with the known biodistribution of [^{18}F]FHBG in normal mice due to hepatobiliary excretion (**Fig. 4d**)[39]. This result was corroborated using tissue extraction and *ex vivo* gamma-counting at day 10 (**Fig. 4g**).

Comparing anti-HER2 SNIPR-PET with anti-HER2 [^{89}Zr]trastuzumab and [^{18}F]FDG. Our newly developed SNIPR T-cell based tool was based on co-localization of cells and antigen, with subsequent identification of tumor allowed by subsequent HSV-tk mediated intracellular trapping of [^{18}F]FHBG. We sought to confirm the specificity of this novel cell-based imaging using currently available immunoPET. Trastuzumab has the same anti-HER2 scFv binding moiety as our SNIPR, thereby reflecting the affinity-based interaction of the same antigen/antibody pair[40]. ^{18}F based labeling is not available for most antibody-based immunoPET because this technology generally requires relatively long incubation time (on the order of days) to achieve ideal tracer biodistribution. We used [^{89}Zr]trastuzumab (anti-HER2) PET-imaging as well as [^{18}F]FDG-PET in the same animal model as SNIPR-CAR system (N = 4). Overall, different biodistributions of the two tracers were observed, consistent with distinct metabolism and excretion pathways (**Fig. 5a**). Both immunoPET with [^{89}Zr]trastuzumab and SNIPR-PET with [^{18}F]FHBG demonstrated statistically significant increased radiotracer enrichment in HER2+ tumor compared to HER2– tumor (9.9 fold with $p<0.001$ and 9.3 fold with $p=0.002$, respectively)(**Fig. 5b**). The relative radiotracer enrichment within HER2+ tumor compared to HER2- tumor was not statistically significant between ImmunoPET and SNIPR-PET ($p > 0.05$) (**Fig. 5c**). Likewise, the relative radiotracer enrichment within HER2+ tumor compared to background was also not statistically significant between ImmunoPET and SNIPR-PET ($p > 0.05$) (**Fig. 5d**). Imaging results using [^{89}Zr]trastuzumab were corroborated via *ex vivo* analysis of harvested tissues (**Supp. Fig. S4**). Although not statistically significant, the trend of higher [^{18}F]FDG accumulation in HER2– tumor compared to HER2+ tumor on a %ID/cc basis correlated with the higher growth rate of MD468 (HER2–) compared to SKBR3 (HER2+) we observed both *in vitro* and *in vivo* (**Fig. 5b, middle and 5d**). In general, the observed [^{18}F]FDG and [^{89}Zr]trastuzumab accumulation in HER2+ and HER2- tumors were consistent with values reported in the literature[41], with variability in [^{89}Zr]trastuzumab signals likely related to differences in obtained molar activity.

SNIPR_PET can be extended to the glioblastoma antigen EGFRvIII. To demonstrate the feasibility of SNIPR-PET in other cancers, we chose glioblastoma-specific antigen EGFRvIII as the next target antigen. EGFRvIII is a constitutively active, ligand-independent mutant of the EGF receptor (EGFR), highly specific to GBMs[42]. EGFRvIII can be found in approximately 20% of glioblastoma cases[43]. Within EGFRvIII+ tumor samples, the proportion of EGFRvIII-expressing cells has been shown to range from 37-86%[44]. We designed T cells to constitutively express SNIPR that targets EGFRvIII and conditionally express CAR that targets distinct antigen, IL13Rα2, analogous to our previous approach for targeting glioblastoma with cytotoxic CD8 T cells[16]. At baseline, those T cells express only anti-EGFRvIII SNIPR, without CAR or reporter. When they recognize EGFRvIII, they express IL13-mutein (IL13m)-CAR that strongly binds to more widely expressed but less specific target interleukin 13 receptor alpha 2 (IL13Rα2), as well as reporter genes (**Fig. 6a**). To demonstrate *in vitro* reporter activation upon anti-EGFRvIII SNIPR activation, we generated three different T cells with Blue Fluorescent Protein (BFP), nano-Luciferase (nLuc) and tkSR39 reporters. Those reporters were co-expressed with IL13m-CAR, and then cleaved at the intervening T2A sequence to generate separate CAR and reporter proteins. By using this strategy, T cells could be generated with two vectors, thereby achieving a higher FACS yield of T cell transduction than the HER2 system. As expected, T cells bearing anti-EGFRvIII SNIPR receptor induced a significantly higher level of BFP and nLuc activity 48 hours after co-culturing with EGFRvIII+ U87 cells, compared to co-culturing with EGFRvIII– U87 cells (BFP: n=4, 25-fold, $p<0.001$; nLuc: n=4, $p=0.002$) (**Fig. 6b, left and middle**). T cells bearing anti-EGFRvIII SNIPR receptor and inducible IL13m-CAR-T2A-tkSR39 demonstrated a significantly higher level of [^{18}F]FHBG uptake when co-cultured with EGFRvIII+ U87 cells compared to the same T cells co-cultured with EGFRvIII– U87 cells (n=8, 32.5 fold, $p<0.001$). To demonstrate the potential for *in vivo* imaging, we again generated a mouse model with EGFRvIII+ U87 and EGFRvIII– U87 xenografts by subcutaneous injection, followed by SNIPR T cell injection and PET imaging for the next 10 days (n = 4) (**Fig. 6c**). ROI analysis demonstrated a significantly higher level of radiotracer within EGFRvIII+ xenograft compared to EGFRvIII– xenograft, which was maximized at day 8, based on per volume radioactivity (%ID/cc) (14 fold, $p<0.001$) (**Fig. 6d and e**). As seen on the HER2 SNIPR-CAR system, EGFRvIII SNIPR CAR system demonstrated a decrease in PET signal at day 10, likely secondary to low target killing activity of activated CD4+ T cells (**Fig. 6d)**. Again, EGFRvIII+ and EGFRvIII- xenografts were sacrificed at day 10 for ex vivo analysis, which confirmed significantly higher enrichment of radiotracer within the EGFRvIII+

xenograft compared to EGFRvIII– xenograft based on per weight radioactivity (%ID/g) (5 fold excess, $p<0.001$) (**Fig. 6e)**.

Discussion:

We have developed an antigen-specific, PET-compatible SNIPR T cell reporter system, in response to the rapidly proliferating interest in T cell-mediated treatment of human tumors. This customizable synthetic receptor platform provides an essential companion to CAR T mediated treatment, reflected by the recent application of synNotch to oncologic challenges[16]. Applying several rounds of synthetic biology, our laboratory has developed antiHER2-SNIPR T cells that (1) are antigen-inducible, as detected by GFP fluorescence, luciferase luminescence, and the HSV-TK PET reporter [^{18}F]FHBG and (2) can be successfully imaged dual xenograft animal models. The key to achieving the novel cell-based imaging technology SNIPR-PET is the sequential signal amplification mechanisms by adopting three synthetic biology breakthroughs into the original synNotch system. *First*, we dramatically increased the efficacy of the synthetic receptor by re-engineering the original synNotch receptor[45]. *Second*, we designed T cells to proliferate within the tumor microenvironment by triggering a conditionally active T cell proliferation signal. Third, we adopted a high-activity mutant thymidine kinase that exhibits over 40 times higher enzymatic activity in trapping [^{18}F]FHBG[46]. Importantly, all three components were necessary to achieve the detection sensitivity required for PET and each signal amplification scheme has significant room for improvement and many more molecular candidates to test, in this versatile system.

We started by demonstrating imaging using anti-HER2 SNIPR, given the prevalence of molecular therapies targeting HER2, as well as related immunoPET imaging tools. After successful demonstration of HER2 SNIPR-PET, we have also developed antigen-inducible SNIPR T cells for EGFRvIII, an important antigen in human glioblastoma. Amplification of EGFR and its gain-of-function mutant EGFRvIII occur frequently in glioblastoma[47]. Among EGFR mutants found in glioblastoma, EGFRvIII occurs most commonly, and represents a late event, occurring after amplification of EGFR-WT. Compared to EGFR-WT, EGFRvIII lacks amino acids 6–273, and deletion of those 268 amino acids creates a junction site with a new glycine residue between amino acids 5 and 274. Epidermal growth factor receptor variant III (EGFRvIII) is considered

a glioblastoma-specific antigen that is present in approximately 30% of glioblastoma patients[48]. We currently see more than 300 patients a year with glioblastoma at UCSF, with EGFRvIII+ tumors therefore representing a significant number of cases. The expression of EGFRvIII confers potential specificity to new treatment approaches, allowing for minimal off-target toxicity, but its heterogeneous expression throughout the tumor remains a difficulty, requiring high-sensitivity imaging. We have recently addressed this challenge via parallel synNotch circuits[16].

The main advantage of SNIPR-PET is in detection of antigen-dependent signals depending on activation of T cells in the tumor microenvironment, for better imaging T cell-based therapies. We also considered the general diagnostic potential of SNIPR-PET T cells given the potential amplification of PET signals in a cell-based approach. In this manuscript, the detection sensitivities of [^{89}Zr]Trastzumab immunoPET and anti-HER2 [^{18}F]FHBG SNIPR PET were similar. However, SNIPR-PET has a great room for enhancing sensitivity, through molecular mechanisms augmenting T cell recognition and proliferation. Expanding the sensitivity of SNIPR-PET via synthetic biology tools is the focus of ongoing work. In its current form, SNIPR-PET is still far from becoming a standalone diagnostic tool because of its complexity and high cost. As engineered T cell mediated therapies mature and are more widely translate into the clinic, we expect this cost would drop, especially with the development of low-cost allogeneic SNIPR T cells. Detection and molecular characterization of early or recurrent tumor in high-risk population, especially for tumors that are risky to biopsy, would be appealing targets for this technology.

In conclusion, we have developed a novel cell-based imaging technology, SNIPR-PET with successful visualization of specific molecular targets *in vivo*. We have demonstrated applicability of this imaging modality to two different tumor antigens- HER2 and EGFRvIII. This technology could be used as a companion biomarker for CAR T therapies, for example to characterize off-target effects, or verify tumor engagement. As the technology matures, SNIPR-PET could be used to detect and characterize molecular profile of early cancers without biopsy.

Methods:

Receptor and Response Element Construct Design

SNIPR receptor design

SNIPRs were built by fusing anti-HER-2 scFvs or anti-EGFRvIII scFvs with a truncated CD8α hinge region (TTTPAPRPPTPAPTIASQPLSLRPEAC), human Notch1 transmembrane domain (FMYVAAAAFVLLFFVGCGVLLS), intracellular Notch2 juxtamembrane domain (KRKRKH), and a Gal4-VP64 transcriptional element. All receptors contain an N-terminal CD8α signal peptide (MALPVTALLLPLALLLHAARP) for membrane targeting and a myc-tag (EQKLISEEDL) for easy determination of surface expression with α-myc AF647 (Cell-Signaling #2233). Four versions of antiHER-2 scFv with different affinities, 4D5-3, 4D5-5, 4D5-7 and 4D5-8[49], and two versions of anti-EGFRviii scFv, 139 and 3C10[50], were tested and 4D5-8 for HER2 system and 139 for EGFRvIII system were used if not otherwise stated. Receptors were cloned into a modified pHR'SIN:CSW vector containing a PGK promoter for all primary T cell experiments.

Chimeric Antigen Receptor (CAR) design

CARs were built by fusing a binding head (anti-HER2 4D5-8 scFv or IL13 mutein), CD8□ transmembrane domain, , co-stimulatory domain 4-1BB, CD3ζ and eGFP. Of note, eGFP in the C terminal of CAR did not affect the function of CAR. All receptors contain an N-terminal CD8α signal peptide (MALPVTALLLPLALLLHAARP) for membrane targeting and FLAG tag (DYKDDDDK) for easy determination of surface expression. The anti-HER2 CAR was cloned into a modified pHR'SIN:CSW vector containing a constitutive pGK promoter for *in vivo* experiments. The IL13-mutein CAR was cloned as inducible vector by cloning into pHR'SIN:CSW that contains five copies of the Gal4 DNA binding domain target sequence (GGAGCACTGTCCTCCGAACG), followed by an inducible CMV promoter. In inducible vectors, IL13 mutein CAR was followed by T2A-HSV-tkSR39 or T2A-nLuc for co-induction with reporter genes. All inducible CAR-T2A-reporter vectors contained constitutively expressed fluorophore genes (mCitrine or mCherry) to easily identify transduced T cells. All induced elements were cloned via a BamHI site in the multiple cloning site 3′ to the Gal4 response elements. All constructs were cloned via In-Fusion cloning (Takara # 638951).

Reporter design

All reporter constructs were cloned into either a modified pHR'SIN:CSW vector containing a Gal4UAS-RE-CMV promoter followed by multiple cloning site, pGK promoter and mCherry or a modified pHR'SIN:CSW

vector containing a Gal4UAS-RE-CMV promoter followed by multiple cloning site, pGK promoter and mCitrine. All reporter-T2A-sIL2 constructs were cloned using pre-existing sIL2 constructs in the lab, stem from pre-existing constructs containing sIL2, based on Levine et al.[35]. HSV-tkSR39-GFP construct was cloned from cEF.tk-GFP (Plasmid #33308, Addgene, MA), which was deposited by Pomper et al. (PubMed ID: 19114988) using site-directed mutagenesis as described in the Supp. Fig. S1a. HSV-tkSR39-T2A-sIL2 construct was cloned from HSV-tkSR39-GFP using In-Fusion cloning (Takara Bio, CA) after adding six C-terminal amino acids (EMGEAN) that were deleted in the original HSV-tk in cEF.tk-GFP, as shown in the Supp. Fig. S1b. nLuc-T2A-sIL2 was cloned from pPRE-pNL1.3 (Plasmid #84394, Addgene, MA). Inducible IL13m-CAR-T2A-reporter constructs were cloned as described above.

Preparation of SNIPR T cells

Primary Human T cell Isolation and Culture

Primary CD4+ and CD8+ T cells were isolated from anonymous donor blood after apheresis by negative selection (STEMCELL Technologies #15062 & 15063). Blood was obtained from Blood Centers of the Pacific (San Francisco, CA) as approved by the University Institutional Review Board. CD4+ T cells and CD8+ T cells were separated using Biolegend MojoSort Human CD4 T Cell Isolation Kit (Biolegend #480130, San Diego, CA) following manufacturer's protocol. In all experiments in this manuscript, we used human CD4+ T cells with minimal target-killing activity. T cells were cryopreserved in RPMI-1640 (Thermo Fisher #11875093) with 20% human AB serum (Valley Biomedical Inc., #HP1022) and 10% DMSO. After thawing, T cells were cultured in human T cell medium consisting of X- VIVO 15 (Lonza #04-418Q), 5% Human AB serum and 10 mM neutralized N-acetyl L- Cysteine (Sigma-Aldrich #A9165) supplemented with 30 units/mL IL-2 (NCI BRB Preclinical Repository) for most experiments. For experiments involving the induction of Super IL-2, primary T-cells were maintained in human T cell media supplemented with IL-2 until experimentation, whereupon media was replaced with media without supplemented IL-2.

Lentiviral Transduction of Human T cells

Pantropic VSV-G pseudotyped lentivirus was produced via transfection of Lenti-X 293T cells (Clontech #11131D) with a pHR'SIN:CSW transgene expression vector and the viral packaging plasmids pCMVdR8.91 and pMD2.G using Mirus Trans-IT Lenti (Mirus #MIR6606). Primary T cells were thawed the same day, and after 24 hours in culture, were stimulated with Human T-Activator CD3/CD28 Dynabeads (Life Technologies #11131D) at a 1:3 cell:bead ratio. At 48 hours, viral supernatant was harvested, and the primary T cells were exposed to the virus for 24 hours. At day 5 post T cell stimulation, the CD3/CD28 Dynabeads were removed, and the T cells were sorted for assays with a Beckton Dickinson (BD) FACs ARIA II. Sorted T-cells were cultured in the T cell media for 24 hours, CD3/CD28 Dynabeads was added at a 1:3 cell:bead ratio to expand for the next 3 days. CD3/CD28 Dynabeads were removed, and the cells were further cultured/expanded for 7 days, at which point, almost all T cells stopped dividing. Those T cells were cryopreserved in RPMI-1640 (Thermo Fisher #11875093) with 20% human AB serum (Valley Biomedical Inc., #HP1022) and 10% DMSO. 7 days before *in vitro* or *in vivo* experiments, the cryopreserved T cells were thawed and cultured in T cell media with CD3/CD28 Dynabeads at a 1:3 cell:bead ratio for the first 3 days, and the beads were removed, and T cells were cultured 4 additional days to use in experiments.

SNIPR T cell design for in vivo imaging

For HER2+ and HER2- xenograft bioluminescence imaging, we generated anti-HER2 SNIPR T cells with three constructs – constitutively expressed anti-HER2(4D5-8) SNIPR, constitutively expressed anti-HER2(4D5-8) CAR and conditionally expressed firefly luciferase (Supplementary Fig. S3a). At baseline, anti-HER2 SNIPR T cells express anti-HER2 SNIPR and anti-HER2 CAR. Upon binding to HER2, they overexpress fLuc through SNIPR activation and proliferate by CAR activation. For HER2+ and HER2- xenograft PET-CT imaging, we generated anti-HER2 SNIPR T cells with three constructs – constitutively expressed anti-HER2(4D5-8) SNIPR, constitutively expressed anti-HER2(4D5-8) CAR and conditionally expressed HSV-tkSR39-T2A-sIL2 (**Fig. 4a**). At baseline, anti-HER2 SNIPR T cells express anti-HER2 SNIPR and anti-HER2 CAR. Upon binding to HER2, they overexpress HSV-tkSR39 and super IL2 by SNIPR activation, and also proliferate by CAR activation.

For EGFRvIII+ and EGFRvIII- xenograft bioluminescence imaging, we generated anti-EGFRvIII SNIPR T cells with two constructs – constitutively expressed anti-EGFRvIII(139) SNIPR and conditionally expressed IL13

mutein CAR-T2A-nanoLuc (**Fig. 6a**). At baseline, anti-EGFRvIII SNIPR T cells express anti-EGFRvIII SNIPR. Upon binding to EGFRvIII, they overexpress IL13 mutein CAR and nanoLuc. For EGFRvIII+ and EVFRvIII- xenograft bioluminescence imaging, we generated anti-EGFRvIII SNIPR T cells with two constructs – constitutively expressed anti-EGFRvIII(139) SNIPR and conditionally expressed anti-IL13m-CAR-HSV-tkSR39. At baseline, anti-EGFRvIII SNIPR T cells express anti-EGFRvIII SNIPR. Upon binding to EGFRvIII, they overexpress IL13 mutein CAR and HSV-tkSR39.

***In vitro* studies**

Cancer cell lines

The cell lines used were 293T (ATCC #CRL-3216), MDA-MB-468 (ATCC #HTB-132, HER2- cells), SKBR3 (ATCC # HTB-30, HER2+ high cells), MCF7 (ATCC # HTB-22, HER2+ low cells), U87-EGFRvIII-negative luciferase and U87 EGFRvIII-positive luciferase (Choe et al., 2021). All cell lines in this manuscript were cultured in filter sterilized DMEM (Sigma D5648) with 10% FBS and 1% Penicillin/Streptomycin stock (ThermoFisher, 10,000 U Penicillin and 10,000 µg/ml Streptomycin).

In vitro fluorophore and luciferase reporter assay

For *in vitro* SNIPR T cell stimulations, $2x10^5$ T cells were co-cultured with $1x10^5$ cancer cells. After mixing the T cells and cancer cells in flat bottom 96-well tissue culture plates, the cells were centrifuged for 1 min at 400xg to force interaction of the cells and the cultures were analyzed at 48-72 hours for reporter expression. Production of fluorophores (GFP and CFP) were assayed using flow cytometry with a BD LSR II and the data were analyzed with FlowJo software (TreeStar). Production of firefly luciferase was assessed with the ONE-glo Luciferase Assay System (Promega #E6110) and production of nanoLuc luciferase was assessed with the Nano-Glo® Luciferase Assay System (Promega #N1110). Bioluminescence was measured with a FlexStation 3 (Molecular Devices).

In vitro radiotracer uptake assay

Radiosyntheses of [^{18}F]FHBG was performed using established techniques, summarized in **Supplementary Fig. S4** and the supplementary methods for radiosynthesis**.** For *in vitro* SNIPR T cell stimulations, 1x10^6 T cells were co-cultured with 5x10^5 cancer cells. After mixing the T cells and cancer cells in 6-well tissue culture plates, the cells were centrifuged for 1 min at 400xg to force interaction of the cells and the cultures were analyzed at 48-72 hours for radiotracer uptake. On the day of radiotracer uptake experiment, T cells and cancer cells were resuspended and 2 µCi of [^{18}F]FHBG was added to each well, and incubated for 3 hours at 37˚C, 5% CO_2. Cells were resuspended and washed three times with 4˚C 2% FBS PBS. The retained radiotracer activity was measured using a Hidex gamma counter (Turku, Finland).

Reporter assays with varying receptor affinity and abundance (Heatmap)

The heatmap for reporter expression was generated with four versions of anti-HER2 SNIPR T cells bearing anti-HER2 SNIPR receptor with varying HER2 binding affinity (4D5-3, 4D5-5, 4D5-7 and 4D5-8 scFv with the order of increasing binding affinity). All the SNIPR T cells had inducible reporter of HSV-tk-GFP fusion protein that is to be detected with flow cytometry. SNIPR T cells were incubated with cancer cells with varying amount of surface HER2 expression (293T, MD468, MCF7 and SKBR3 with the order of increasing HER2 expression levels). 2x10^5 SNIPR T cells were co-cultured with 1x10^5 cancer cells in flat bottom 96-well tissue culture plates for 48-72 hours and the production of HSV-tk-GFP was assayed using flow cytometry with a BD LSR II and the data were analyzed with FlowJo software (TreeStar).

The heatmap for radiotracer accumulation was generated with three versions of anti-HER2 SNIPR T cells bearing anti-HER2 SNIPR receptor with varying HER2 binding affinity (4D5-5, 4D5-7 and 4D5-8 scFv). All the SNIPR T cells had reporter of HSV-tk-T2A-sIL2 protein. SNIPR T cells were incubated with cancer cells with varying amount of surface HER2 expression (293T, MCF7 and SKBR3 with the order of increasing HER2 expression levels). 1x10^6 SNIPR T cells were co-cultured with 5x10^5 cancer cells in flat bottom 6-well tissue culture plates for 48-72 hours. The FHBG radiotracer uptake was measured using a Hidex gamma counter.

***In vivo* studies**

Murine models/ tumor cohorts studied:

All mouse experiments were conducted according to Institutional Animal Care and Use Committee (IACUC)–approved protocols. Both luciferase-based and PET reporter data were acquired, and two dual xenograft models were studied. After determining the optimal timepoint using optical imaging, (8-10 days), PET imaging was then performed at several time points with sacrifice to verify tissue tracer accumulation (gamma counting) and perform histology and antigen staining[51–53].

Optical Imaging:

As shown in **Supp. Fig. S3**, luciferase-based studies were performed initially (21 days) to investigate the optimal timepoint for [^{18}F]FHBG detection of T-cell induction. The SNIPR-T cell distribution within tumor was determined by luminescence emission using a Xenogen IVIS Spectrum after intravenous D-luciferin injection according to the manufacturer's directions (GoldBio).

PET imaging:

Radiosyntheses of [^{18}F]FHBG, [^{18}F]FDG and [^{89}Zr]trastzumab: Radiosyntheses of [^{18}F]FHBG, [^{18}F]FDG and [^{89}Zr]trastzumab were performed as described in the supplementary methods.

Imaging protocol: The same general imaging protocol was used for all studies. A tail vein catheter was placed in mice under isoflurane anesthesia and the radio tracer was subsequently injected. The animals were placed on a heating pad to minimize shivering. Mice were allowed to recover and micturate, and at specific later time point, the animals were again anesthetized under isoflurane and transferred to a Siemens Inveon micro PET-CT system (Siemens, Erlangen, Germany), and imaged using a single static 25 min PET acquisition followed by a 10 min micro-CT scan for attenuation correction and anatomical co-registration. No adverse events were observed during or after injection of any compound. Anesthesia was maintained during imaging using isofluorane.

[^{18}F]FHBG SNIPR model: Two murine models were studied: (1) a dual HER2+/ HER2- flank model (n = 7) and (2) a dual EGFRvIII+/ EGFRvIII- flank model (n = 4). For the HER2+/HER2– dual xenograft model, 4 x 10^6 SKBR3 cells and 1 x 10^6 MD468 cells were implanted subcutaneously into 6-10 week-old female NCG mice (Charles River). For the EGFRvIII+/EGFRvIII– dual xenograft model, 1 x 10^6 EGFRvIII+ or EGFRvIII– U87 cells were implanted subcutaneously into 6-10 week-old female NCG mice (Charles River). All mice were then injected with 6.0 × 10^6 SNIPR T cells intravenously via tail vein in 100 µl of PBS. For PET imaging, 150 mCi of [^{18}F]FHBG was administered via tail vein. At 1 h post-injection, imaging was acquired on day 3, 6, 8, 10 post T cell injection. Upon completion of imaging on day 10, mice were sacrificed, and biodistribution analysis was performed. Gamma counting of harvested tissues was performed using a Hidex Automatic Gamma Counter (Turku, Finland).

[^{18}F]FDG model: The HER2+/HER2– dual xenograft model was developed as previously described; 4 x 10^6 SKBR3 cells and 1 x 10^6 MD468 cells were implanted subcutaneously into 6-10 week-old female NCG mice (Charles River), with 4 mice per group. For PET imaging, 150 uCi of [^{18}F]FDG was administered via tail vein. At 1 h post-injection, imaging was acquired.

[^{89}Zr]trastuzumab model: The same [^{18}F]FDG cohort was used (n = 4). For PET imaging, 150 uCi of [^{89}Zr]trastuzumab was administered via tail vein. At 3 days post-injection, imaging was acquired. Upon completion of imaging, mice were sacrificed, and biodistribution analysis was performed. Gamma counting of harvested tissues was performed using a Hidex Automatic Gamma Counter (Turku, Finland).

Data analysis and statistical methods

FACS analysis data were processed using FlowJo (BD biosciences, NJ). For representing data, all graphs are depicted with error bars corresponding to the standard error of the mean. All statistical analysis of *in vitro* data was performed using Microsoft Excel, program language R (https://www.R-project.org/) and Prism software version 7.0 (GraphPad, CA). Data was analyzed using one-way analysis of variance tests (ANOVA) and/or unpaired two-tailed Student's t-test. PET/µCT data was analyzed using the open source software AMIDE[54] and

%ID/v was used for quantitative comparison. A 95% confidence interval was used to distinguish significant differences in all cases.

References:

1. Larson, R. C. & Maus, M. V. Recent advances and discoveries in the mechanisms and functions of CAR T cells. *Nat. Rev. Cancer* **21,** 145–161 (2021).
2. Frey, N. V. Chimeric antigen receptor T cells for acute lymphoblastic leukemia. *Am. J. Hematol.* **94,** S24–S27 (2019).
3. Laetsch, T. W. Chimeric antigen receptor T-cell therapy for acute lymphocytic leukaemia: where are we in 2020? *Lancet Haematol.* **7,** e778–e779 (2020).
4. Tang, X.-J. *et al.* Therapeutic potential of CAR-T cell-derived exosomes: a cell-free modality for targeted cancer therapy. *Oncotarget* **6,** 44179–44190 (2015).
5. van der Stegen, S. J. C., Hamieh, M. & Sadelain, M. The pharmacology of second-generation chimeric antigen receptors. *Nat. Rev. Drug Discov.* **14,** 499–509 (2015).
6. Brudno, J. N. & Kochenderfer, J. N. Chimeric antigen receptor T-cell therapies for lymphoma. *Nat. Rev. Clin. Oncol.* **15,** 31–46 (2018).
7. Xin Yu, J., Hubbard-Lucey, V. M. & Tang, J. The global pipeline of cell therapies for cancer. *Nat. Rev. Drug Discov.* **18,** 821–822 (2019).
8. Mikkilineni, L. & Kochenderfer, J. N. Chimeric antigen receptor T-cell therapies for multiple myeloma. *Blood* **130,** 2594–2602 (2017).
9. Morgan, R. A. *et al.* Case report of a serious adverse event following the administration of T cells transduced with a chimeric antigen receptor recognizing ERBB2. *Mol. Ther.* **18,** 843–851 (2010).
10. Linette, G. P. *et al.* Cardiovascular toxicity and titin cross-reactivity of affinity-enhanced T cells in myeloma and melanoma. *Blood* **122,** 863–871 (2013).
11. Cameron, B. J. *et al.* Identification of a Titin-derived HLA-A1-presented peptide as a cross-reactive target for engineered MAGE A3-directed T cells. *Sci. Transl. Med.* **5,** 197ra103 (2013).
12. Morsut, L. *et al.* Engineering customized cell sensing and response behaviors using synthetic notch receptors. *Cell* **164,** 780–791 (2016).
13. Roybal, K. T. *et al.* Precision Tumor Recognition by T Cells With Combinatorial Antigen-Sensing Circuits. *Cell* **164,** 770–779 (2016).
14. Roybal, K. T. *et al.* Engineering T Cells with Customized Therapeutic Response Programs Using Synthetic Notch Receptors. *Cell* **167,** 419–432.e16 (2016).
15. Zhu, I. *et al.* Design and modular assembly of synthetic intramembrane proteolysis receptors for custom gene regulation in therapeutic cells. *BioRxiv* (2021). doi:10.1101/2021.05.21.445218
16. Choe, J. H. *et al.* SynNotch-CAR T cells overcome challenges of specificity, heterogeneity, and persistence in treating glioblastoma. *Sci. Transl. Med.* **13,** (2021).
17. Hyrenius-Wittsten, A. *et al.* SynNotch CAR circuits enhance solid tumor recognition and promote persistent antitumor activity in mouse models. *Sci. Transl. Med.* **13,** (2021).
18. Heskamp, S. *et al.* 89Zr-Immuno-Positron Emission Tomography in Oncology: State-of-the-Art 89Zr Radiochemistry. *Bioconjug. Chem.* **28,** 2211–2223 (2017).
19. Wei, W. *et al.* Immunopet: concept, design, and applications. *Chem. Rev.* **120,** 3787–3851 (2020).
20. Mestel, R. Cancer: Imaging with antibodies. *Nature* **543,** 743–746 (2017).
21. Aalipour, A. *et al.* Engineered immune cells as highly sensitive cancer diagnostics. *Nat. Biotechnol.* **37,** 531–539 (2019).
22. Zhang, L. *et al.* Macrophages: friend or foe in idiopathic pulmonary fibrosis? *Respir. Res.* **19,** 170 (2018).
23. Rőszer, T. Understanding the Mysterious M2 Macrophage through Activation Markers and Effector Mechanisms. *Mediators Inflamm.* **2015,** 816460 (2015).
24. Kuchimaru, T. *et al.* A luciferin analogue generating near-infrared bioluminescence achieves highly sensitive deep-tissue imaging. *Nat. Commun.* **7,** 11856 (2016).
25. Chu, J. *et al.* A bright cyan-excitable orange fluorescent protein facilitates dual-emission microscopy and enhances bioluminescence imaging in vivo. *Nat. Biotechnol.* **34,** 760–767 (2016).
26. Zhu, I. *et al.* Design and modular assembly of synthetic intramembrane proteolysis receptors for custom

gene regulation in therapeutic cells. *BioRxiv* (2021). doi:10.1101/2021.05.21.445218
27. Pomper, M. G. *et al.* Serial imaging of human embryonic stem-cell engraftment and teratoma formation in live mouse models. *Cell Res.* **19,** 370–379 (2009).
28. Black, M. E., Kokoris, M. S. & Sabo, P. Herpes simplex virus-1 thymidine kinase mutants created by semi-random sequence mutagenesis improve prodrug-mediated tumor cell killing. *Cancer Res.* **61,** 3022–3026 (2001).
29. Rabinovich, B. A. *et al.* Visualizing fewer than 10 mouse T cells with an enhanced firefly luciferase in immunocompetent mouse models of cancer. *Proc. Natl. Acad. Sci. USA* **105,** 14342–14346 (2008).
30. Rainov, N. G. A phase III clinical evaluation of herpes simplex virus type 1 thymidine kinase and ganciclovir gene therapy as an adjuvant to surgical resection and radiation in adults with previously untreated glioblastoma multiforme. *Hum. Gene Ther.* **11,** 2389–2401 (2000).
31. Yaghoubi, S. *et al.* Human pharmacokinetic and dosimetry studies of [(18)F]FHBG: a reporter probe for imaging herpes simplex virus type-1 thymidine kinase reporter gene expression. *J. Nucl. Med.* **42,** 1225–1234 (2001).
32. Yaghoubi, S. S. & Gambhir, S. S. PET imaging of herpes simplex virus type 1 thymidine kinase (HSV1-tk) or mutant HSV1-sr39tk reporter gene expression in mice and humans using [18F]FHBG. *Nat. Protoc.* **1,** 3069–3075 (2006).
33. Ghaffari, S. *et al.* Optimizing interleukin-2 concentration, seeding density and bead-to-cell ratio of T-cell expansion for adoptive immunotherapy. *BMC Immunol.* **22,** 43 (2021).
34. Ross, S. H. & Cantrell, D. A. Signaling and Function of Interleukin-2 in T Lymphocytes. *Annu. Rev. Immunol.* **36,** 411–433 (2018).
35. Levin, A. M. *et al.* Exploiting a natural conformational switch to engineer an interleukin-2 “superkine”. *Nature* **484,** 529–533 (2012).
36. Kim, J. H. *et al.* High cleavage efficiency of a 2A peptide derived from porcine teschovirus-1 in human cell lines, zebrafish and mice. *PLoS One* **6,** e18556 (2011).
37. Parker, M. F. L. *et al.* Sensing Living Bacteria in Vivo Using d-Alanine-Derived 11C Radiotracers. *ACS Cent. Sci.* **6,** 155–165 (2020).
38. Parker, M. *et al.* Cyclic gallium-68 labeled peptides for specific detection of human angiotensin-converting enzyme 2. *J. Nucl. Med.* (2021). doi:10.2967/jnumed.120.261768
39. Campbell, D. O. *et al.* Structure-guided engineering of human thymidine kinase 2 as a positron emission tomography reporter gene for enhanced phosphorylation of non-natural thymidine analog reporter probe. *J. Biol. Chem.* **287,** 446–454 (2012).
40. Dijkers, E. C. *et al.* Biodistribution of 89Zr-trastuzumab and PET imaging of HER2-positive lesions in patients with metastatic breast cancer. *Clin. Pharmacol. Ther.* **87,** 586–592 (2010).
41. Al-Saden, N., Cai, Z. & Reilly, R. M. Tumor uptake and tumor/blood ratios for 89Zr-DFO-trastuzumab-DM1 on microPET/CT images in NOD/SCID mice with human breast cancer xenografts are directly correlated with HER2 expression and response to trastuzumab-DM1. *Nucl Med Biol* **67,** 43–51 (2018).
42. Huang, P. H. *et al.* Quantitative analysis of EGFRvIII cellular signaling networks reveals a combinatorial therapeutic strategy for glioblastoma. *Proc. Natl. Acad. Sci. USA* **104,** 12867–12872 (2007).
43. Moscatello, D. K. *et al.* Frequent expression of a mutant epidermal growth factor receptor in multiple human tumors. *Cancer Res.* **55,** 5536–5539 (1995).
44. Wikstrand, C. J., McLendon, R. E., Friedman, A. H. & Bigner, D. D. Cell surface localization and density of the tumor-associated variant of the epidermal growth factor receptor, EGFRvIII. *Cancer Res.* **57,** 4130–4140 (1997).
45. Zhu, I. *et al.* Design and modular assembly of synthetic intramembrane proteolysis receptors for custom gene regulation in therapeutic cells. *BioRxiv* (2021). doi:10.1101/2021.05.21.445218
46. Sundaram, G. S. M., Harpstrite, S. E., Kao, J. L.-F., Collins, S. D. & Sharma, V. A new nucleoside analogue with potent activity against mutant sr39 herpes simplex virus-1 (HSV-1) thymidine kinase (TK). *Org. Lett.* **14,** 3568–3571 (2012).
47. An, Z., Aksoy, O., Zheng, T., Fan, Q.-W. & Weiss, W. A. Epidermal growth factor receptor and EGFRvIII in glioblastoma: signaling pathways and targeted therapies. *Oncogene* **37,** 1561–1575 (2018).
48. Vengoji, R. *et al.* Afatinib and Temozolomide combination inhibits tumorigenesis by targeting EGFRvIII-cMet signaling in glioblastoma cells. *J Exp Clin Cancer Res* **38,** 266 (2019).
49. Carter, P. *et al.* Humanization of an anti-p185HER2 antibody for human cancer therapy. *Proc. Natl. Acad. Sci. USA* **89,** 4285–4289 (1992).
50. Morgan, R. A. *et al.* Recognition of glioma stem cells by genetically modified T cells targeting EGFRvIII

and development of adoptive cell therapy for glioma. *Hum. Gene Ther.* **23,** 1043–1053 (2012).
51. Aldape, K. D. *et al.* Immunohistochemical detection of EGFRvIII in high malignancy grade astrocytomas and evaluation of prognostic significance. *J. Neuropathol. Exp. Neurol.* **63,** 700–707 (2004).
52. Felsberg, J. *et al.* Epidermal Growth Factor Receptor Variant III (EGFRvIII) Positivity in EGFR-Amplified Glioblastomas: Prognostic Role and Comparison between Primary and Recurrent Tumors. *Clin. Cancer Res.* **23,** 6846–6855 (2017).
53. Gupta, P. *et al.* Development of an EGFRvIII specific recombinant antibody. *BMC Biotechnol.* **10,** 72 (2010).
54. Loening, A. M. & Gambhir, S. S. AMIDE: a free software tool for multimodality medical image analysis. *Mol. Imaging* **2,** 131–137 (2003).
55. Zhao, Y. *et al.* A herceptin-based chimeric antigen receptor with modified signaling domains leads to enhanced survival of transduced T lymphocytes and antitumor activity. *J. Immunol.* **183,** 5563–5574 (2009).
56. Becker, K. F. *et al.* Quantitative protein analysis from formalin-fixed tissues: implications for translational clinical research and nanoscale molecular diagnosis. *J. Pathol.* **211,** 370–378 (2007).

Acknowledgements: Grant sponsors NIH (R01-EB024014, R01-EB025985); Kleberg Foundation 132472B; Society of Interventional Radiology.The authors would also like to thank Dr. Suzanne E. Lapi for providing [^{89}Zr]trastuzumab.

Author contributions: J.S., K.T.R., D.M.W. and T.D.T. proposed and supervised the overall project. J.B. performed or supported the radiochemistry. J.S., I.Z., R.L., and C.I.R. generated the receptor and reporter constructs and generated SNIPR T cells. P.B.W. and H.O. generated EGFRvIII+ and EGFRvIII- cell lines. M.F.L.P. generated HER2 and EGFRvIII xenografts. M.F.L.P., A.A., J.L. and M.K. performed the *in vitro* PET studies. M.F.L.P. and A.A. performed μPET-CT imaging studies and J.S., M.F.L.P. and R.F. performed subsequent data analysis. M.F.L.P. and A.A. performed *ex vivo* analysis. C.I.R. and T.D.T performed histology analysis of *ex vivo* specimens. J.S., K.T.R. and D.M.W. wrote and edited the paper.

Competing interests: I.Z. and K.T.R. are co-inventors on patents for synthetic receptors (PRV 62/905,258, 62/905,262, 62/905,266, 62/905,268, 62/905,251, 62/905,263). K.T.R. is a cofounder of Arsenal Biosciences, consultant, SAB member, and stockholder. K.T.R. is an inventor on patents for synthetic Notch receptors (WO2016138034A1, PRV/2016/62/333,106) and receives licensing fees and royalties. The patents were licensed by Cell Design Labs and are now part of Gilead. He was a founding scientist/consultant and stockholder in Cell Design Labs, now a Gilead Company. K.T.R. holds stock in Gilead. K.T.R. is on the SAB of Ziopharm Oncology and an Advisor to Venrock.

Materials and Correspondence:

*E-mail: kole.roybal@ucsf.edu
*E-mail: david.m.wilson@ucsf.edu
*E-mail: thea.tlsty@ucsf.edu

Supplementary information: Please see the supplementary information for detailed information regarding molecular biology, radiosynthesis, and several imaging studies not reported in the main text.

Figures:

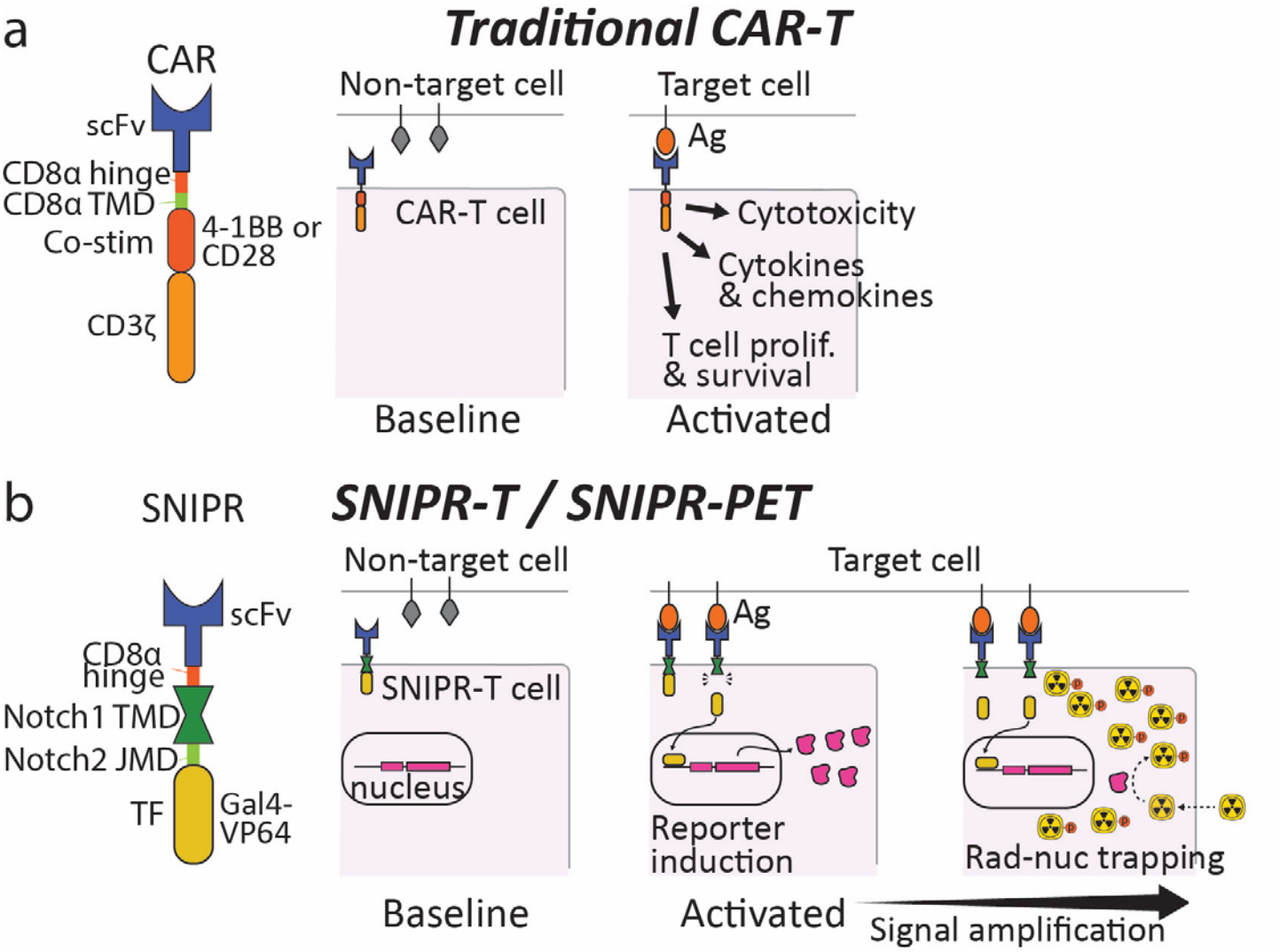

Fig. 1 | SNIPR-T cells and SNIPR-PET, in comparison to traditional chimeric antigen rector (CAR)-T cells. A CAR comprises an extracellular antigen recognition domain (scFv), CD8□ hinge domain and CD8□ transmembrane domain (TMD), co-stimulatory domains (Co-stim) such as 4-1BB or CC28 and a CD3ζ domain.

When scFv of CAR binds to its target antigen, intracellular domains trigger a native T cell response. The native T cell response includes cytotoxicity, cytokines, chemokine and growth factor secretion, and T cell proliferation and survival. B. SNIPR consists of an extracellular antigen recognition domain (scFv), CD8□ hinge domain, Notch1 TMD, Notch2 Juxtamembrane domain (JMD) and transcription factor (TF) domain Gal4. When scFv of SNIPR binds to its target antigen, TMD is cleaved and TF falls off from the receptor, entering the nucleus to activate pre-programmed gene expression. In this example, SNIPR activates the expression of PET reporter genes (middle). The overexpressed proteins trap PET radiotracers, visible on PET/CT. Since radiotracer accumulation benefits from enzyme turnover, the signal from scFv-Ag binding is potentially amplified.

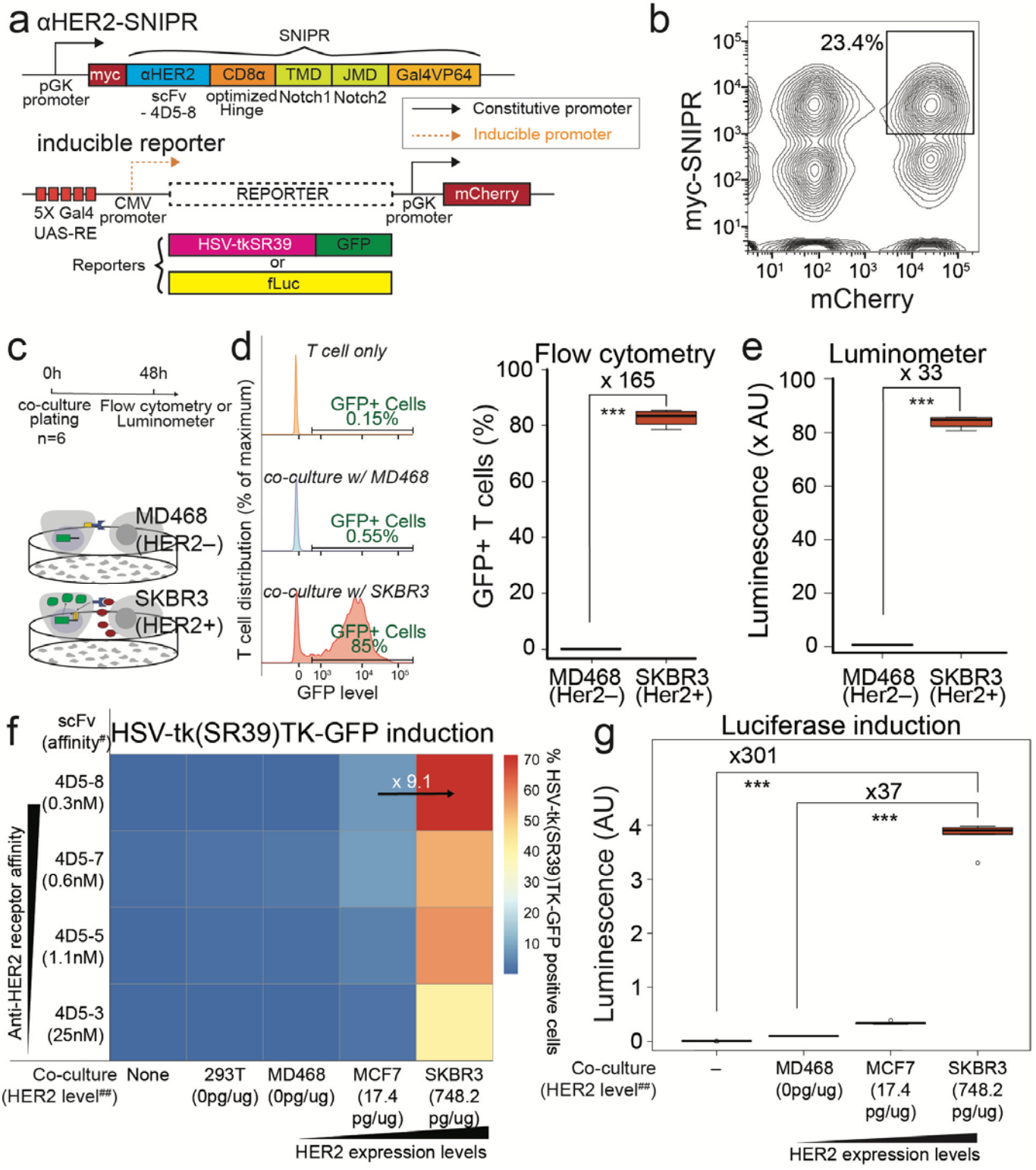

Fig. 2 | Anti-HER2-SNIPR activation and reporter expression. a. To demonstrate the feasibility of SNIPR-PET, we engineered T cells capable of SNIPR-induced thymidine kinase expression and SNIPR-induced luciferase enzymatic activity. We generated cells bearing an anti-HER2 SNIPR and inducible HSV-tkSR39-GFP or inducible luciferase reporters. Anti-HER2-SNIPR have a myc-tag, which is a short peptide that can be stained for cell sorting. The reporter plasmids contain constitutively expressed mCherry fluorescent protein,

which is also used for cell sorting. SNIPR T cells are generated by double transduction using lentivirus. b. T cells expressing both SNIPR and mCherry are sorted using fluorescence activated cell sorting (FACS). The double positive T cells were about 15-50%. c. SNIPR T cells are co-cultured with either MD468 (HER2– cells, negative control) or SKBR3 (HER2+ cells) for 48 hours d. TK-GFP reporter expression is detected using FAC analysis. An example of FAC analysis for TK-GFP expression is shown, in anti-HER2 SNIPR T cells only (top, left), anti-HER2 SNIPR T cells with HER2- cells (middle, left) and anti-HER2 SNIPR T cells with HER2+ cells (bottom, left). There was an over 150-fold increase in number of HSV-tkSR39-GFP+ cells after incubating with SKBR3 (HER2+) compared to after incubating with MD468 (HER2-)(right). e. Activation of antiHER2-SNIPR induced an over 33-fold increase in luciferase enzymatic activity after incubating with SKBR3 (HER2+) compared to after incubating with MD468 (HER2-). f. We tested the effect of receptor binding affinity and target antigen abundance to HSV-tkSR39-GFP induction by using anti-HER2 SNIPR cells with varying HER2 binding affinities, and by using cancer cells with varying levels of HER2 expression. As expected, increasing the HER2 binding affinity of SNIPR receptor and increasing HER2 abundance resulted in higher induction of HSV-tkSR39-GFP. g. We tested the effect of increasing target antigen abundance to the SNIPR-induced luciferase enzymatic activity. Increasing target antigen abundance demonstrated a higher level of luciferase enzymatic activity. *$p<0.05$, **$p<0.01$, ***$p<0.001$. #scFv affinity values from Zhao et al.[55], ##HER2 abundance values from Becker et al.[56].

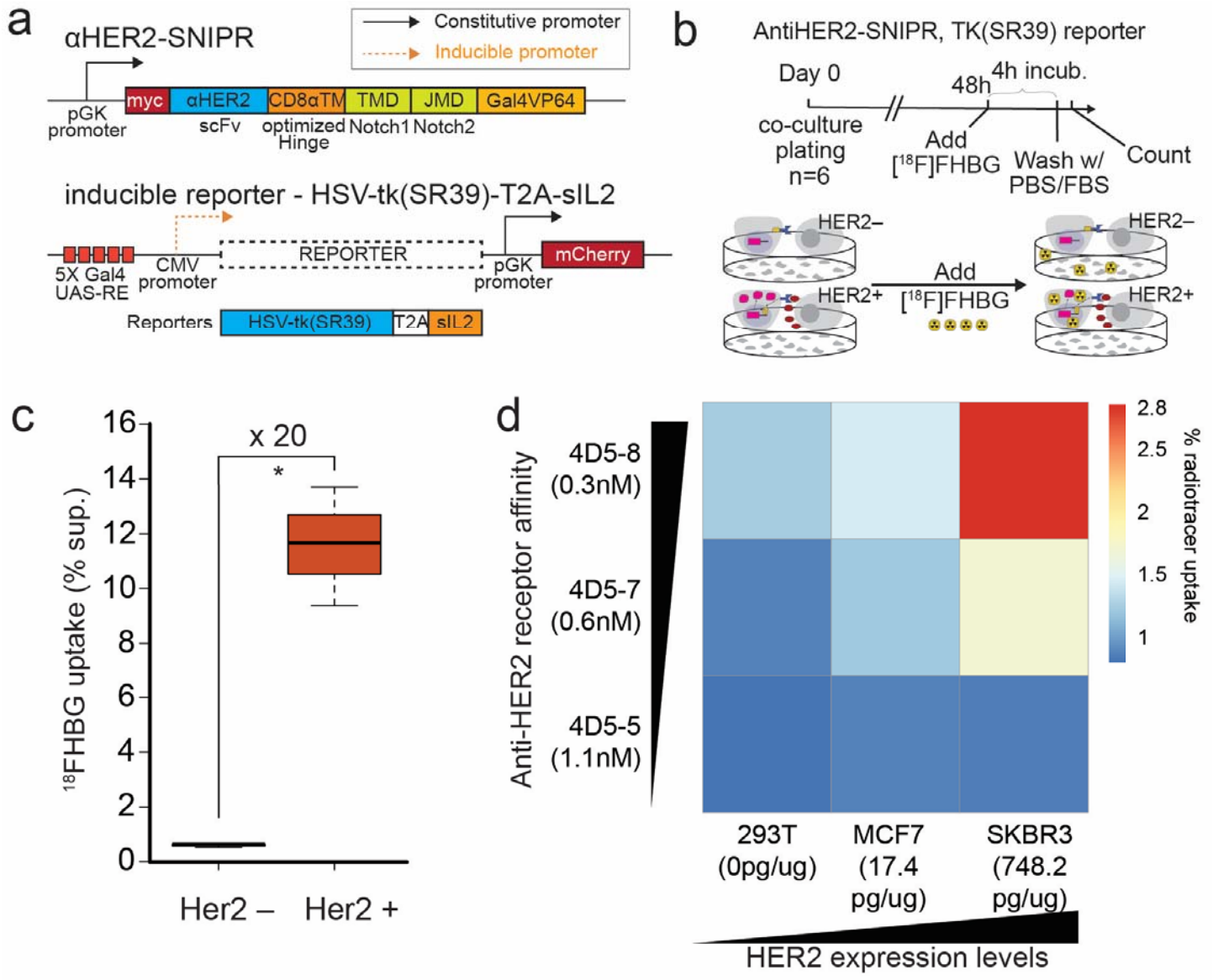

Fig. 3 | *In vitro* [^{18}F]FHBG uptake in activated anti-HER2 SNIPR T cells. a. Constructs that were used for the *in vitro* SNIPR-induced [^{18}F]FHBG uptake experiment. We generated T cells bearing an anti-HER2 SNIPR receptor and inducible HSV-tk(SR39)-T2A-sIL2, followed by FACS with myc and mCherry. b. Anti-HER2 SNIPR T cells were co-cultured with HER2+ (SKBR3) or HER2- (MD468) cells for 48 hours, followed by 3 hour incubation with [^{18}F]FHBG. Retained radioactivity was measured after washing the cells to remove extracellular [^{18}F]FHBG. c. SNIPR T cells co-cultured with HER2+ (SKBR3) cells accumulated significantly higher amount of [^{18}F]FHBG radiotracer compared to T cells co-cultured with HER2– (MD468) cells. d. Similar to **Fig. 2f**, we tested the effect of receptor binding affinity and target antigen abundance on [^{18}F]FHBG accumulation by using anti-HER2 SNIPR with varying HER2 binding affinities, and by using cancer cells with varying levels of HER2 expression. As expected, increasing HER2 binding affinity of SNIPR receptor and increasing HER2 abundance resulted in greater enrichment of [^{18}F]FHBG. *p<0.05, **p<0.01, ***p<0.001.

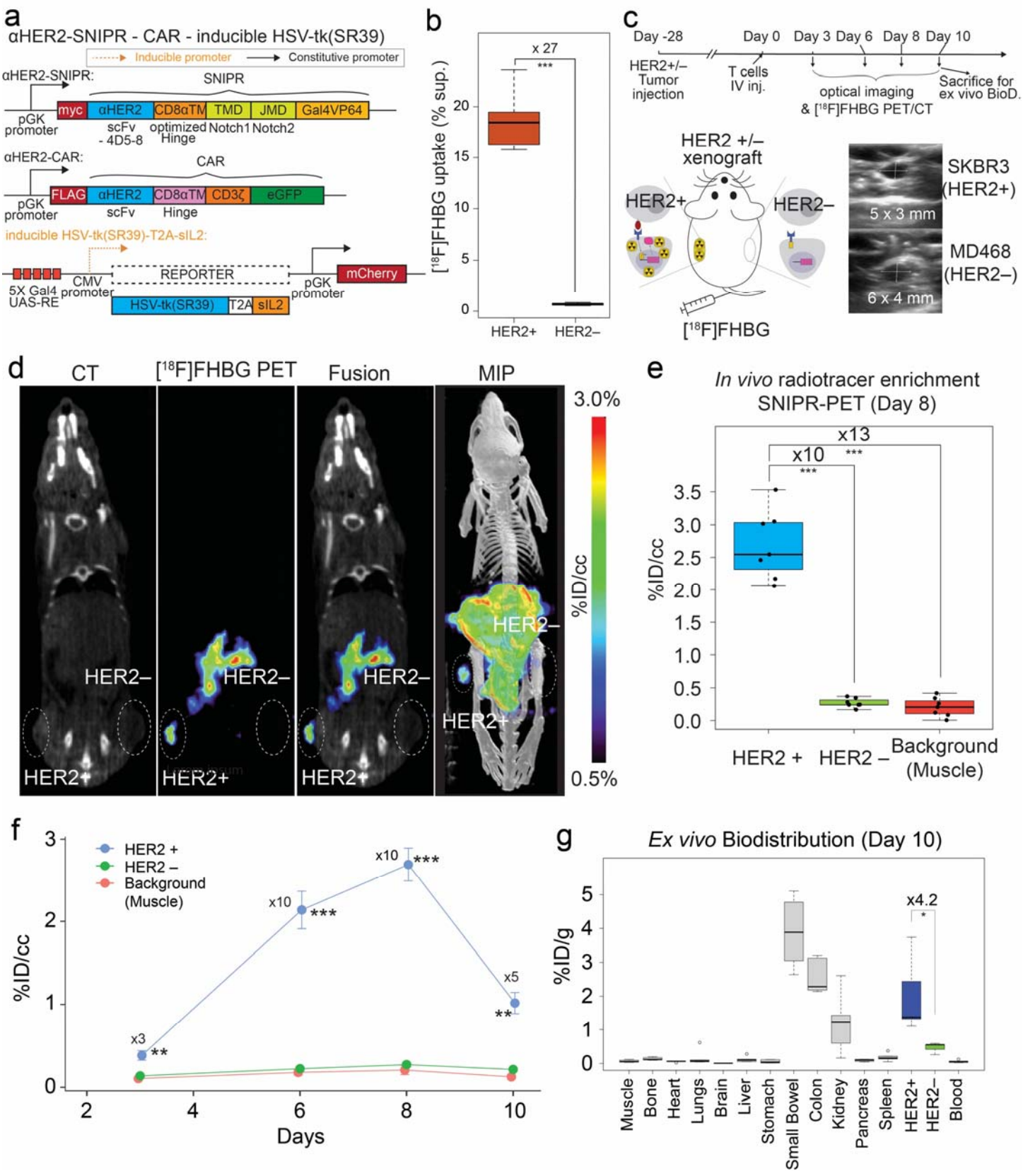

Fig. 4 | *In vivo* [^{18}F]FHBG uptake in HER2+ tumors using activated anti-HER2 SNIPR T cells. a. For PET-CT, we generated T cells by transducing three plasmids including anti-HER2 SNIPR, anti-HER2 CAR and

inducible HSV-tk(SR39)-T2A-sIL2, followed by FACS using myc, GFP and mCherry. b. We repeated the *in vitro* radiotracer accumulation of activated SNIPR T cells also bearing CAR, following the experimental scheme shown in the **Fig. 3b.** We confirmed significantly higher ^{18}FHBG accumulation in SNIPR T cells after co-culturing with SKBR3 (HER2+) cells compared to MD468 (HER2–) cells. c. Double xenograft mouse models were generated by implanting SKBR3(HER2+) and MD468 (HER2–) cells in left and right flank soft tissue. 4 weeks after tumor implantation, SNIPR T cells were injected into tail veins. Micro-PET/CT was acquired 3 days, 6 days, 8 days and 10 days after T cell injection. d. Representative image of [^{18}F]FHBG PET-CT demonstrates similar size of xenografts with radiotracer enrichment only within SKBR3 (HER2+) xenograft and not within MD468 (HER2–) xenograft. Significant radiotracer was also visualized within bowel, likely due to hepatobiliary secretion of [^{18}F]FHBG tracer. e. Quantitative ROI analysis of the HER2+ and HER2– tumors and background (shoulder muscle) demonstrates statistically significant radiotracer enrichment within the HER2+ xenograft, 10 times and 13 times greater than within the HER2– xenograft and background. f. Time-dependent ROI analysis of radiotracer enrichment within the HER2+ tumor demonstrates the greatest radiotracer enrichment at day 8 post T cell injection. Slightly decreased radiotracer enrichment was observed at day 10, at which point the mice were sacrificed for ex vivo analysis. g. Biodistribution analysis (day 10) of [^{18}F]FHBG enrichment within different organs demonstrated significantly greater [^{18}F]FHBG enrichment within HER2+ xenograft compared to HER2– xenograft. As seen on microPET-CT, the GI system demonstrated a high level of [^{18}F]FHBG uptake. *$p<0.05$, **$p<0.01$, ***$p<0.001$.

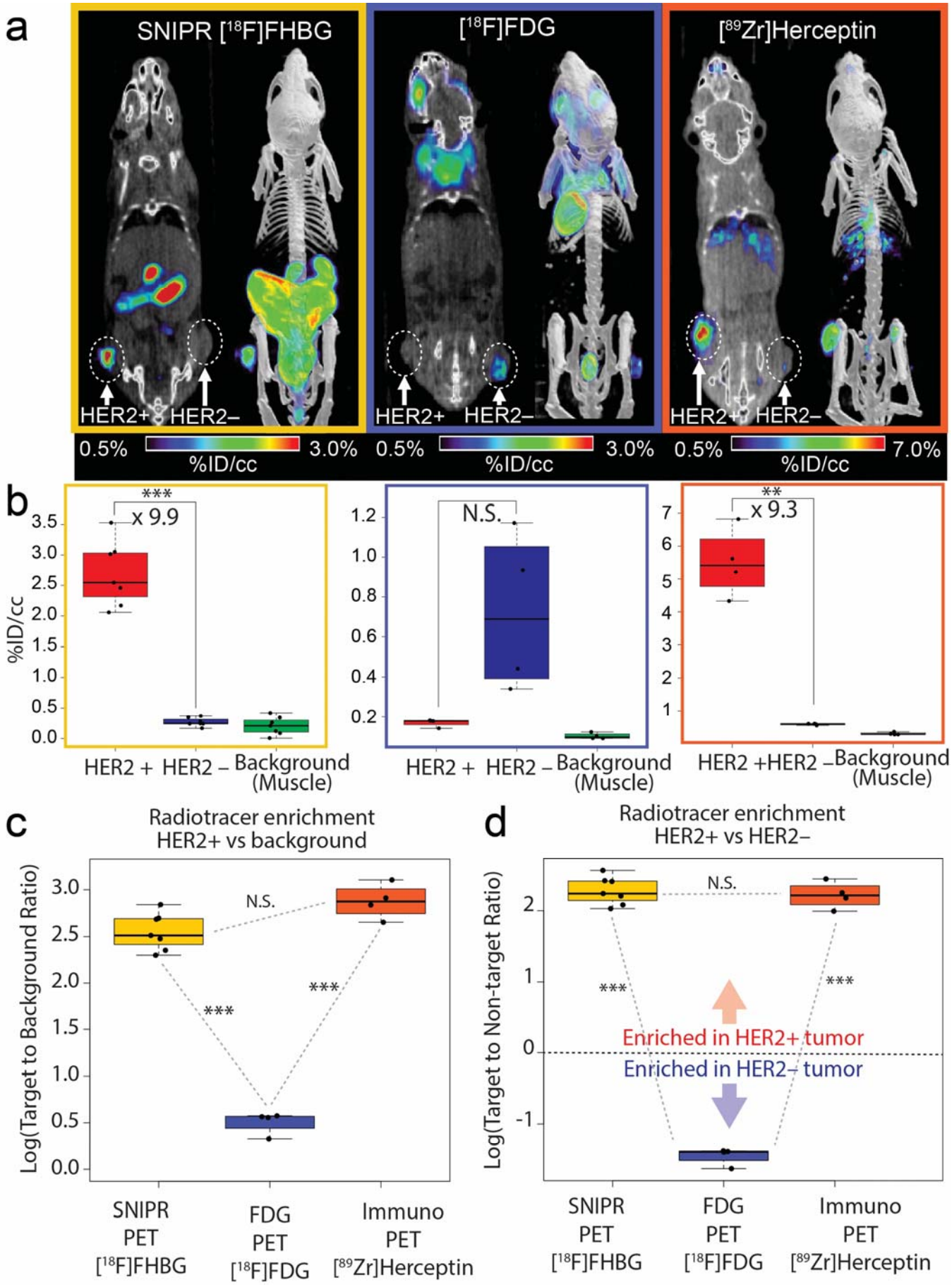

Fig. 5 | Comparison between SNIPR-PET, FDG-PET and ImmunoPET. a. Representative images of

[^{18}F]FHBG SNIPR-PET, [^{18}F]FDG-PET and [^{89}Zr]-herceptin-PET. SNIPR-PET and Herceptin immunoPET demonstrated radiotracer enrichment within SKBR3(HER2+) xenograft compared to MD468 (HER2–) tumor, whereas FDG-PET demonstrated higher radiotracer enrichment within MD468 tumor. b. ROI analysis demonstrated statistically significant, 9.9-fold greater enrichment of [^{18}F]FHBG within HER2+ tumor than within HER2– tumor (left), non-statistically significant enrichment (p-value > 0.05) of FDG within HER2– tumor compared to HER2+ tumor, and statistically significant 9.3 times greater enrichment of [^{89}Zr]Herceptin within HER2+ tumor than within HER2– tumor. c and d. Fold enrichment of radiotracer within HER2+ tumor was significantly greater in SNIPR-PET and ImmunoPET compared to FDG-PET, when compared to background (c) and when compared to HER2– tumor (d). *p<0.05, **p<0.01, ***p<0.001.

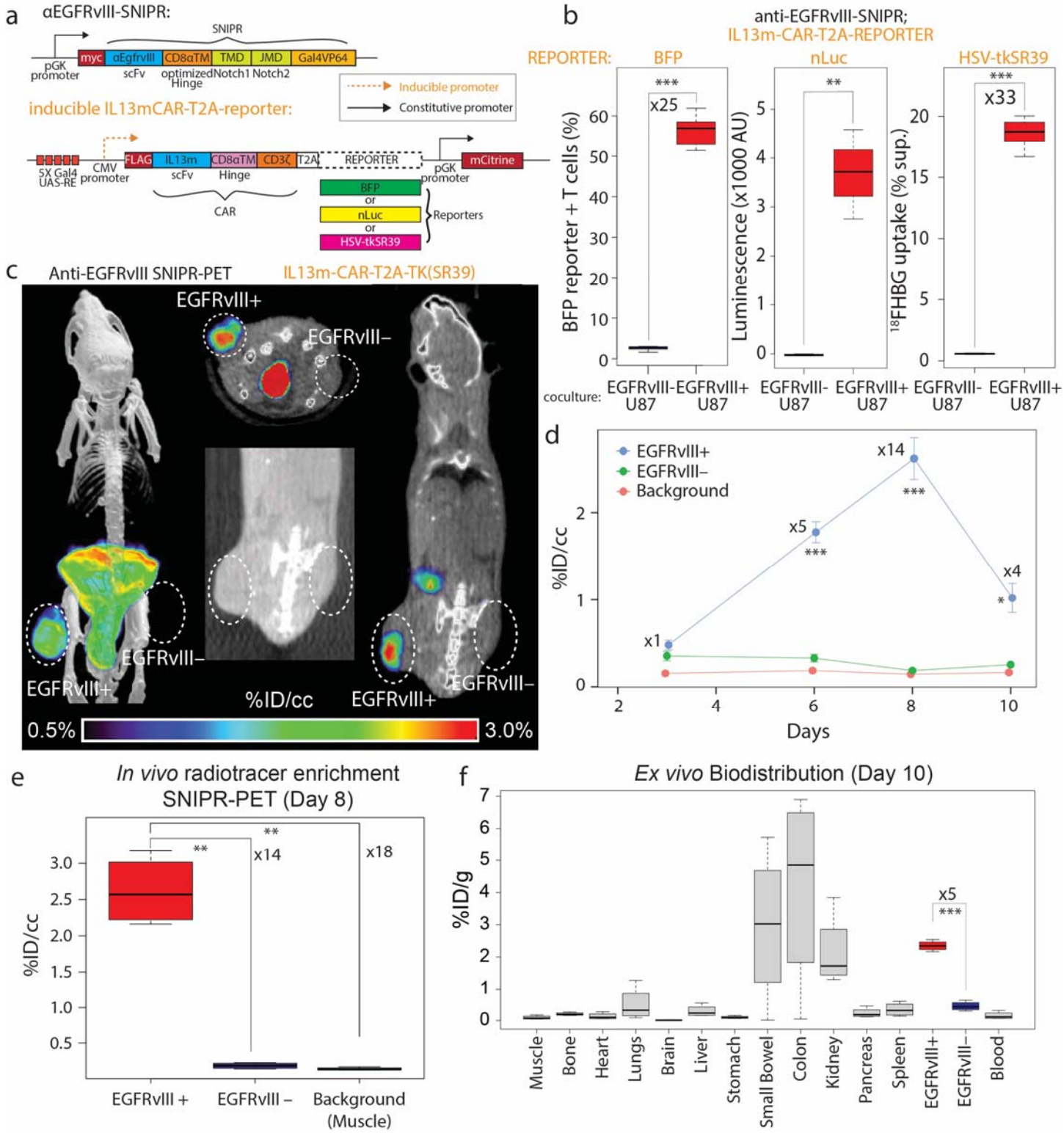

Fig. 6 | EGFRvIII SNIPR-PET. a. We generated SNIPR-T cells with anti-EGFRvIII-SNIPR and inducible IL13-mutein (IL13m)-CAR-T2A-reporter constructs. We used three different reporters – Blue Fluorescent Protein (BFP), nanoLuc (nLuc) and HSV-tkSR39. In this system, SNIPR T cells express anti-EGFRvIII-SNIPR at baseline but do not express IL13m-CAR or reporters. When anti-EGFRvIII binds to EGFRvIII on target cells, SNIPR T cells now induce the expression of IL13m-CAR and reporters - BFP, nLuc or HSV-tkSR39. Since

most U87 cells express IL13Rα2, T cells expressing IL13m-CAR now secrete cytokines and growth factors that induce T cell proliferation and survival. b. SNIPR T cells incubated with EGFRvIII+ U87 cells demonstrated significantly higher level of BFP reporter expression, significantly greater level of nLuc enzymatic activity and HSV-tkSR39-mediated ^{18}FHBG accumulation compared to SNIPR T cells incubated with EGFRvIII– U87 cells. c. Following a similar protocol as used for HER2, EGFRvIII+ U87 and EGFRvIII– U87 cells were implanted into mouse flank subcutaneous tissues. 4 weeks after implantation, anti-EGFRvIII T cells with inducible anti-IL13-mutein-CAR-T2A-HSV-tk(SR39) were injected into the tail veins. 3 days, 6 days, 8 days and 10 days after T cell injection, the mice were analyzed with PET-CT after injecting ^{18}FHBG into the tail vein. Representative PET-CT at day 8 demonstrates high radiotracer enrichment within the EGFRvIII+ U87 xenograft compared to the EGFRvIII– U87 xenograft on the contra-lateral side. d. Time dependent ROI analysis of radiotracer enrichment within the EGFRvIII+ xenograft demonstrates the greatest radiotracer enrichment at day 8 post T cell injection, followed by slight decrease in PET signal at day 10, at which point, animals were sacrificed for ex vivo biodistribution analysis. e. Quantitative ROI analysis of the EGFRvIII+ and EGFRvIII– tumors and background (shoulder muscle) demonstrate statistically significant radiotracer enrichment within the EGFRvIII+ xenograft, 14 times and 18 times greater than within the EGFRvIII– xenograft and background. f. *Ex vivo* analysis (day 10) of [^{18}F]FHBG enrichment within different organs demonstrated significantly greater [^{18}F]FHBG enrichment within EGFRvIII+ xenograft compared to EGFRvIII– xenograft. As seen on microPET-CT images, the GI system demonstrated a high level of [^{18}F]FHBG. *$p<0.05$, **$p<0.01$, ***$p<0.001$.